

Activated carbon developed from orange peels: Batch and dynamic competitive adsorption of basic dyes



Maria Emilia Fernandez ^{a,b}, Gisel Vanesa Nunell ^{a,b}, Pablo Ricardo Bonelli ^{a,b},
Ana Lea Cukierman ^{a,b,c,*}

^a Programa de Investigación y Desarrollo de Fuentes Alternativas de Materias Primas y Energía – PINMATE, Departamento de Industrias, Facultad de Ciencias Exactas y Naturales, Universidad de Buenos Aires, Intendente Güiraldes 2620, Ciudad Universitaria, C1428BGA Buenos Aires, Argentina

^b Consejo Nacional de Investigaciones Científicas y Técnicas (CONICET), Av. Rivadavia 1917, C1033AAJ Buenos Aires, Argentina

^c Cátedra de Farmacotecnia II, Departamento de Tecnología Farmacéutica, Facultad de Farmacia y Bioquímica, Universidad de Buenos Aires, Junín 956, C1113AAD Buenos Aires, Argentina

ARTICLE INFO

Article history:

Received 24 April 2014

Received in revised form 14 August 2014

Accepted 7 September 2014

Keywords:

Orange peel-based activated carbon

Phosphoric acid activation

Basic dyes removal

Binary equilibrium isotherms

Competitive dynamic adsorption

ABSTRACT

Activated carbon from orange (*Citrus sinensis*) peel was developed through H₃PO₄ acid activation. Its ability as an adsorbent for the removal of two representative basic dyes (methylene blue and rhodamine B) from single and binary dyes solutions in batch and continuous modes was examined. The orange peel-based activated carbon presented a high specific surface area (1090 m²/g), predominance of mesopores and acidic character. It also showed a high adsorption capacity for both dyes in batch and dynamic modes. Experimental equilibrium isotherms obtained from single-dye solutions fitted the Langmuir–Freundlich model, and those obtained from binary solutions were properly described by single and multi-component models. Breakthrough curves obtained from single-dye solutions exhibited a better removal performance for rhodamine B. Adsorption capacity at exhaustion time for this dye was 11% higher than for methylene blue. Additional experiments in dynamic conditions with a binary solution of both dyes pointed to adsorption competition for the active sites of the developed carbon. Breakthrough curves were adequately represented by a modified two-parameter model.

© 2014 Elsevier B.V. All rights reserved.

1. Introduction

Among wastewaters treatment methods, adsorption using activated carbons (ACs) has been found superior to others in terms of initial costs and simplicity of design and operation (Wawrzkiewicz and Hubicki, 2009). ACs are successfully proven adsorbents employed nowadays for the full-scale treatment of wastewaters, mainly for its efficiency and ease of implementation (Benadjemia et al., 2011). However, because of the elevated cost of production, available agricultural solid wastes are being intensively investigated for the production of low cost effective ACs. The conversion of waste materials into ACs adds economic value, helps reduce the cost of waste disposal, and provides a potentially less expensive alternative to the existing commercial samples

(Rafatullah et al., 2010). Orange peels are one of these valuable waste materials discarded from juice industry. Since world orange production is estimated in more than 60 millions tons (Siles López et al., 2010) and a significant fraction is destined to industrialization, land space occupation and pollution with phenolic compounds due to dumping of the waste, are becoming problematic (El Nemr et al., 2009).

In addition, watercourses are threatened by a large number of toxic compounds. Among them, about 10% of the hundreds of thousands tons of dyes produced annually worldwide may be found in wastewaters and their complex aromatic molecular structures make them very stable and difficult to biodegrade (Deniz et al., 2011; Rodríguez Couto, 2009). Numerous studies are focused on adsorption of dyes from single-component systems (Dutta et al., 2011; Hao et al., 2010). However, effluents are a mixture of several contaminants, and available data on possible enhancing or inhibitory effects on the adsorption of dyes in a mixed system is limited (Janaki et al., 2012). Moreover, sometimes the data acquired in batch mode are not applicable to treatment systems where contact time is not sufficient to attain equilibrium, and then continuous adsorption studies are needed (Lodeiro et al., 2006). So far, only

* Corresponding author at: PINMATE, Departamento de Industrias, Facultad de Ciencias Exactas y Naturales, Universidad de Buenos Aires, Intendente Güiraldes 2620, Ciudad Universitaria, C1428BGA Buenos Aires, Argentina.

Tel.: +54 11 45763383; fax: +54 11 45763366.

E-mail address: analea@di.fcen.uba.ar (A.L. Cukierman).

few studies have focused on the conversion of orange peels into ACs and their ability to remove dyes (El Nemr et al., 2009; Foo and Hameed, 2012), and there is no precedent of any orange peel-based AC investigated as an adsorbent for mixtures of dyes in batch and continuous modes.

Within this framework, the present work focuses on the development of an activated carbon using orange peel through chemical activation with H_3PO_4 acid and the examination of the feasibility of using it as an adsorbent for the removal of two representative basic dyes, methylene blue (MB) and rhodamine B (RhB), from single and binary solutions in batch and continuous modes. This is a closer approach to real wastewater since it considers the simultaneous co-existence of two dyes. The physicochemical and textural characteristics of the developed carbon were evaluated and compared with those of the precursor. The effects of main operational parameters were examined to optimize removal process variables. Kinetic and equilibrium adsorption parameters were obtained from the application of mathematical models to experimental data. Finally, continuous removal of both dyes was assessed through experiments in an up-flow column.

2. Materials and methods

2.1. Materials

Oranges (*Citrus sinensis*) were purchased from a local fruit market, washed with tap water to eliminate dust and other residues and peeled. The orange peels were cut in small pieces and dried at 60 °C. The dried samples were then crushed, milled and further rinsed with warm water, dried again and finally screen-sieved. The precursor material obtained is hereafter abbreviated as OPP. The fraction of particle diameter between 500 and 1000 μm was selected for the preparation of the activated carbon.

Two basic dyes of analytical grade were used for the adsorption experiments: methylene blue (basic blue 9, C.I. 52015, M.W. 373.91 g/mol) purchased from Carlo Erba®, and rhodamine B (basic violet 10, C.I. 45170, M.W. 479.02 g/mol), purchased from Sigma-Aldrich®. Analytical grade H_3PO_4 acid was purchased from Biopack®.

2.2. Preparation of the activated carbon

An OPP sample was mixed with a 50 wt.% H_3PO_4 acid solution, in a 2:1 acid/precursor weight ratio, and allowed to soak for 2 h at 110 °C. Afterwards, the impregnated sample was placed in a stainless steel fixed-bed reactor heated by an electrical furnace. The temperature was raised from room temperature up to 475 °C at a heating rate of 3 °C/min and held for 0.5 h. Selection of the former conditions was based on previous findings for other precursors (Basso et al., 2002; de Celis et al., 2009). After cooling to room temperature, the sample was soaked in an alkaline solution for 10 min and subsequently rinsed with hot water until a neutral pH was attained. Finally, distilled water was used to complete the rinse. A test using a lead nitrate solution was performed to check for any residual, free, or loosely bound phosphate which could affect further uptake assays (Basso et al., 2002). The sample was then dried in an oven to constant weight, and the yield was evaluated. The developed activated carbon is hereafter abbreviated as OPAC. Yields of 33% were attained.

2.3. Characterization of OPP and OPAC

The fraction of particle diameter between 250 and 500 μm was selected for the characterization of the precursor and the adsorbent. Proximate analysis was performed by thermogravimetric analysis (TA Instruments SDT Q600), according to the American Society of

Testing and Materials' (ASTM) 5142 standards. An automatic elemental analyzer (Carlo Erba model EA 1108) was used to assess their elemental composition.

The total and individual amounts of acidic/polar oxygen functional groups (TOFGs), i.e. carbonyls, phenols, lactones, and carboxyl groups, on the surface of the developed OPAC were determined by titration, following a modified procedure based on Boehm's method (de Celis et al., 2009), and employing solutions of sodium ethoxide, sodium hydroxide and sodium bicarbonate. Likewise, total basic surface groups (TBGs) were determined, following the procedure described in Nunell et al. (2012) and employing a HCl solution. Average values expressed as milliequivalents per gram of sample are reported. Identification of surface functionalities of OPP and OPAC was complementary conducted by Fourier transformed infrared (FT-IR) spectroscopy. The spectra were recorded by transmission method, using a Perkin-Elmer IR Spectrum BXII spectrometer within the range 600–4000 cm^{-1} . Each sample was ground with KBr at an approximate ratio of 1:200 and the resulting mixture was then pressed. The pH of point of zero charge (pH_{PZC}) for OPAC was assessed following the procedure depicted in detail in our previous study (Fernandez et al., 2010).

N_2 adsorption–desorption isotherms at –196 °C for OPP and OPAC were determined with an automatic Micromeritics ASAP-2020 HV volumetric sorption analyzer. Prior to gas adsorption measurements, the dried samples were outgassed at 60 °C (for OPP) and 120 °C (for OPAC) overnight. Textural properties were assessed from the isotherms, according to conventional procedures (Nunell et al., 2012). The Brunauer–Emmett–Teller (BET) surface area (S_{BET}) was determined by the standard BET procedure and total pore volume (V_t) was estimated from the amount of nitrogen adsorbed at the relative pressure of 0.95 ($p/p_0 = 0.95$). The mean pore width (W) was calculated from $W = 4V_t/S_{\text{BET}}$. Pore size distribution (PSD) of the activated carbon was calculated from N_2 adsorption data using the DFT Plus Software (Micromeritics Instrument Corporation), based on the non-local density functional theory (Puzy et al., 2007).

Scanning electron microscopy (SEM) was performed in a Zeiss Supra 40 microscope equipped with a field emission gun and coupled with an energy dispersive spectrometer (EDS, Oxford-instrument Inca x-sight). The images were taken with an in-lens detector and 3 kV acceleration voltages. The samples were placed on an aluminum holder, supported on conductive carbon tape and sputter coated.

2.4. Batch experiments

Stock solutions of 2.1 mmol/L were prepared by dissolving the necessary amount of methylene blue and rhodamine B in distilled water and diluted to obtain the desired concentrations of the dyes. Adsorption experiments were carried out using capped Erlenmeyer flasks in a batch thermostatized system (Lauda Ecoline E200) at 20 ± 0.5 °C, under a wrist-action shaker agitation at a constant speed of 250 rpm up to equilibrium. Afterwards, all samples were centrifuged for 10 min at 5000 rpm and the concentration of each dye was calculated from the measured absorbance in the supernatant at their corresponding maximum absorption wavelength ($\lambda_{\text{max}}\text{MB} = 663 \text{ nm}$ and $\lambda_{\text{max}}\text{RhB} = 553 \text{ nm}$) by means of an UV–vis spectrophotometer (Shimadzu Model UV mini 1240). The fraction of particle diameter between 250 and 500 μm was selected for most batch experiments, with the exception of kinetic experiments, where the fraction between 105 and 250 μm was used, to avoid external and intraparticle mass transfer resistances.

The pH effect on dyes adsorption was studied in the range 2–10. Dyes solutions of alkaline pH were prepared using buffers because it was difficult to maintain these pH values throughout the experiments duration. Solutions of the remaining pH were prepared with distilled water and adjusted with HCl and NaOH solutions. Amounts

of 0.04 g of OPAC were contacted with 100 mL of 0.21 mmol/L MB and RhB solutions, respectively, for 48 h to ensure equilibrium. Dyes removal percentages were calculated as follows:

$$\text{Removal [\%]} = 100 \left(\frac{C_0 - C_e}{C_0} \right) \quad (1)$$

where C_0 and C_e are the initial and equilibrium dye concentrations in solution [mmol/L], respectively.

Kinetic experiments were performed by agitating 0.2 g of OPAC with 100 mL of 0.21 mmol/L MB and RhB solutions, individually, at the same constant speed and at the temperature mentioned above. The pH of the solution was selected as the optimum from the pH effect experiments. Samples were withdrawn at appropriate time intervals and absorbance in the supernatant was measured.

Equilibrium adsorption isotherms from single solutions were obtained by contacting 0.04 g of OPAC with 100 mL of MB or RhB solutions of different initial concentrations (0.08–1.9 mmol/L), until equilibrium was attained. The adsorption isotherms from binary solutions were determined using a ratio of dyes concentrations of 1:1. The same temperature and agitation conditions as well as the pH selected were employed. The amount of dye adsorbed per gram of adsorbent at equilibrium, q_e [mmol/g], was calculated as follows:

$$q_e = \frac{(C_0 - C_e)V}{m} \quad (2)$$

where C_0 is the initial concentration of the dye in the solution [mmol/L], C_e , the equilibrium concentration of dye in the solution [mmol/L], V , the volume of solution [L], and m , the mass of OPAC used [g].

All experiments were performed at least twice. Average values are reported. Solutes and adsorbent blanks were simultaneously run for control under the same conditions.

2.5. Dynamic adsorption from single and binary dyes solutions

For continuous adsorption experiments, a column (1.6 cm internal diameter and 34 cm height) was packed with a known mass of OPAC. The fraction of particle diameter between 105 and 250 μm was used. Prior to the measurements, the bed was washed with distilled water in order to remove all interstitial air. To complete the volume of the column, glass beads were also packed and metallic sieves in the extremes were used to avoid loss of material. The column was then fed with single or binary solutions of MB and RhB of a known concentration (0.21 mmol/L) for each dye, in up-flow mode. The solutions pH was selected from the batch experiments. Dyes solutions were prepared using a Na/K phosphates buffer in order to maintain constant pH 7 throughout the runs. A flow rate of 11 mL/min was adjusted using a peristaltic pump (Masterflex 1–100 rpm, Cole-Parmer) with a flow controller. Samples were collected at the exit of the column at desired time intervals, using a solenoid valve and an automatic sample collector; the dye concentrations were analyzed spectrophotometrically. As earlier described, all the experiments were carried out at $20 \pm 0.5^\circ\text{C}$ using a thermostabilized system (Lauda Ecoline E 300). Temperature was further monitored by an internal thermocouple connected to a digital controller (Iea, Micro 80). The breakthrough time t_b (the time at which the dye concentration in the effluent reached 5% of the influent concentration) and the exhaustion time t_e (the time at which the dye concentration in the effluent reached 95% of the influent concentration) were determined to characterize the breakthrough curves (Fernandez et al., 2010).

Table 1

Proximate and ultimate analyses of the precursor (OPP) and the activated carbon developed (OPAC).

	OPP	OPAC
Proximate analysis ^a [wt.%]		
Volatile matter	73.7	14.9
Ash	3.9	3.4
Fixed carbon ^b	22.4	81.7
Ultimate analysis ^c [wt.%]		
Carbon	43.0	82.5
Hydrogen	5.9	2.5
Nitrogen	0.9	0.9
Sulfur	0.0	0.0
Oxygen ^b	50.2	14.1

^a Dry basis.

^b Estimated by difference.

^c Dry and ash-free basis

3. Results and discussion

3.1. Characterization of OPP and OPAC

Table 1 shows comparatively the physicochemical characteristics of the precursor and the developed activated carbon. As expected, the content of fixed and elemental carbon drastically increased in OPAC in comparison to OPP due to the chemical changes undergone through the process which facilitates the removal of elemental hydrogen and oxygen. The content of volatile matter was reduced in OPAC as a consequence of its release during the thermal treatment stage involved in the activation process.

The adsorption capacity of an activated carbon for a given contaminant is related to its textural properties and the chemical nature of its surface. Chemical characteristics of OPAC are presented in **Table 2**. The pH_{pzc} indicates the acidic nature of the orange peel-based carbon, which is consistent with the pronouncedly higher content of acidic groups in comparison with that of basic surface functionalities. OPAC showed major amounts of phenols and lactones, suggesting a preferential development of this type of functionalities upon activation, and minor contents of carboxylic groups, likely because they begin to decompose at temperatures over 250 °C and become unstable at the temperature used in the thermal treatment stage (de Celis et al., 2009). To appreciate the effect caused on the surface functionalities of the precursor as a consequence of the activation process in more detail, FT-IR spectra of OPP and OPAC samples are presented in Fig. 1. OPP showed numerous characteristic peaks, also reported

Table 2

Chemical characteristics and textural properties of OPAC.

pH _{pzc} ^a	5.5
Surface functional groups [mequiv./g]	
TBGs ^b	0.19
TOFGs ^c	1.46
Carbonyls	0.44
Carboxyls	0.16
Phenols and lactones	0.86
Textural properties	
S_{BET} ^d [m ² /g]	1090
V_t ^e [cm ³ /g]	1.2
V_p ^f [%]	19.7
W_g [nm]	4.3

^a pH of point of zero charge.

^b Total basic groups.

^c Total and individual contents of polar/oxygen functional groups.

^d BET surface area.

^e Total pore volume.

^f Micropore volume determined by DFT method.

^g Mean pore width.

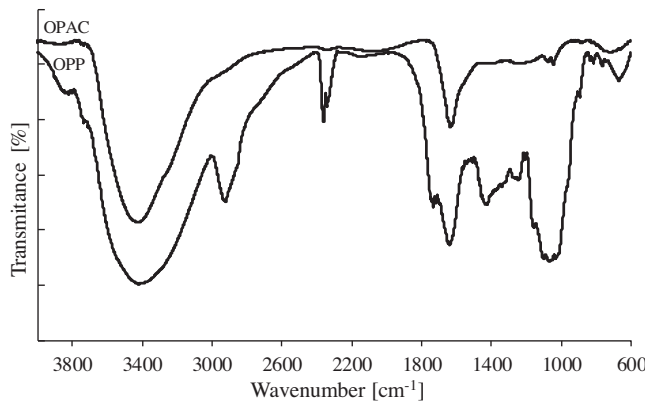


Fig. 1. FT-IR spectra of the precursor (OPP) and the derived activated carbon (OPAC).

by other authors (Thirumavalavan et al., 2011; Feng et al., 2009). OPAC spectrum showed lack of the absorption peaks at 2940 cm⁻¹ and in the region 850–690 cm⁻¹, related to the stretching vibrations of aliphatic and aromatic C–H bonds, respectively. This suggests a lower content of substituting aliphatic groups in the aromatic rings which might be related to the lower content of elemental H determined for the precursor (de Celis et al., 2009). There is a missing small peak at 1736 cm⁻¹, which may be related to the decomposition of carboxylic groups at relatively low temperatures. The lack of peaks in the fingerprint region could be due to the decomposition and cracking of a great number of structures present in the precursor. Some absorption peaks were preserved in OPAC. The intense broad peak around 3430 cm⁻¹ which may be assigned to the stretching vibrations of H-bonded hydroxyl groups from carboxyls, phenols or alcohols and chemisorbed water, and a major peak at 1636 cm⁻¹ corresponding to stretching vibrations of compounds containing carboxylate groups. The peak at 1070 cm⁻¹ could be due to P⁺–O⁻ in acid phosphate esters and to the symmetrical vibration in polyphosphate chain P–O–P, and the band at 1100 cm⁻¹ could be assigned to stretching vibrations of C–O–C in aromatic esters (Puzy et al., 2007).

The photographs obtained by SEM for the precursor and the orange peel-based carbon are presented in Fig. 2a and b. OPP showed flattened walls and large, irregular intercellular spaces; the surface was rough and had an undulating and depressed appearance, consistent with the loss of water from the fresh tissue (Agustí et al., 2001). The directional patterns of the vessels in OPP were conserved in OPAC, and some residual structure of the cell wall could be recognized. It presented a considerable thickness with smooth walls and defined edges. Conducts of different sizes and shapes were observed. This suggests the rearrangement of the structure of the orange peel during the activation. The presence of P detected by EDS in OPAC and not in OPP (data not shown) may be due to P atoms bonded to local oxygenated surface groups or C atoms during the activation process (Benadjemia et al., 2011).

N₂ adsorption/desorption isotherms for the precursor and the activated carbon are illustrated in Fig. 3. The volume of N₂ adsorbed per sample mass unit are represented as a function of the relative pressure (p/p_0), where p is the equilibrium pressure, and p_0 , the saturation pressure of the adsorbate at –196 °C. The adsorption isotherm of OPP presented essentially a type II shape, according to the IUPAC classification, which is typical for non-porous solids (Sangwichien et al., 2002), while the adsorption isotherm for OPAC showed combined characteristics between type I at very low p/p_0 and type II at high p/p_0 , disclosing the simultaneous presence of micropores (<2 nm) and mesopores (2–50 nm). This was confirmed by the presence of the desorption hysteresis loop (H₃/H₄ type), associated to slit-shaped pores (Hu et al., 2001). Details of textural

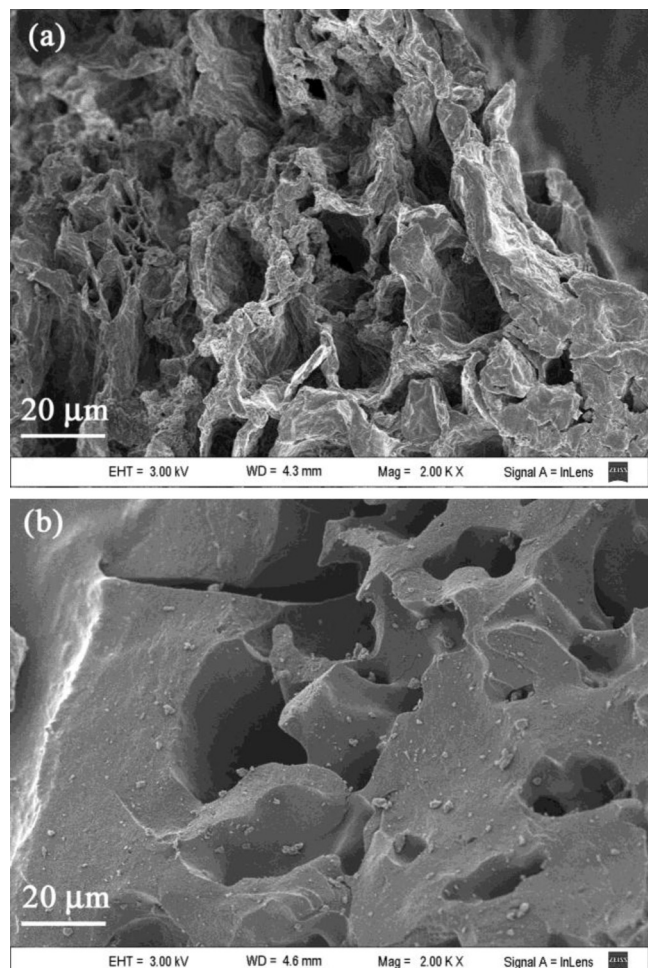


Fig. 2. SEM micrographs at 2000× of magnification for (a) the precursor (OPP) and (b) the activated carbon (OPAC).

parameters of the OPAC, evaluated from isotherms analysis by the Brunauer–Emmett–Teller (BET) and the DFT methods, are reported in Table 2. The BET surface area and the total pore volume were higher for the activated carbon compared to the precursor (1.1 m²/g and 1.2 × 10^{–3} cm³/g, respectively), all of this pointing to a pronounced pore development during the treatment. As reported for the activation process of other lignocellulosic precursors, the

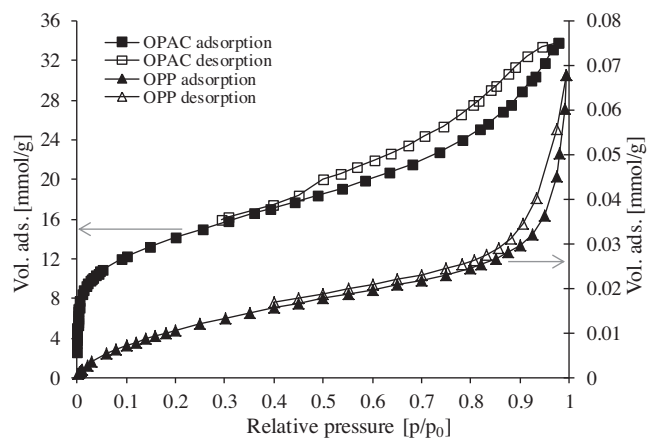


Fig. 3. N₂ adsorption (solid symbols) and desorption (empty symbols) isotherms onto the precursor (OPP) and the activated carbon (OPAC) developed from orange peels.

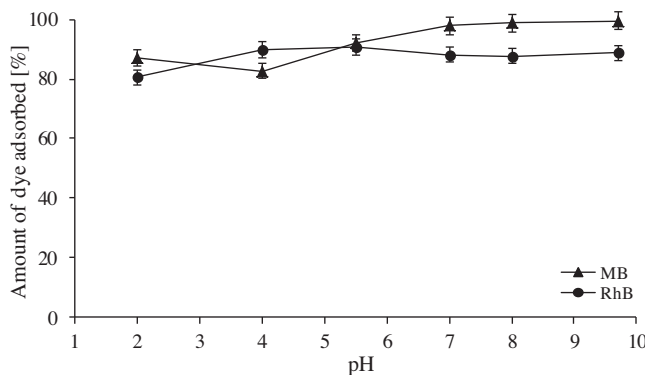


Fig. 4. Effect of the solution's pH on the adsorption of methylene blue (MB) and rhodamine B (RhB) for OPAC at equilibrium. $C_0 = 0.21 \text{ mmol/L}$, dose: $0.04 \text{ g}/100 \text{ mL}$.

H_3PO_4 acid reacting with the internal cellulose structure induces a depolymerization leading to an enhancement of the pore volume and, thus, a global volume expansion (Benadjemia et al., 2011). OPAC was found predominantly mesoporous, as inferred from the low micropore volume shown in Table 2.

3.2. Batch adsorption of the dyes onto OPAC

The variation in the adsorption of MB and RhB onto OPAC was studied in the pH range 2–10 and the results are shown in Fig. 4. It was found that the adsorption efficiency of neither dye was substantially influenced by the solution pH. Nevertheless, a small increase in MB adsorption was observed at solution pH over the pH_{pzc} , suggesting that the adsorbate surface negatively charged increased the electrostatic attraction between positive adsorbate MB and OPAC particles to some extent, enhancing its removal. Minor influence of the solution pH was also obtained for MB adsorption onto activated carbon prepared from oil palm shells (Tan et al., 2008a) and treated sawdust (Garg et al., 2004), and for RhB adsorption onto acid treated commercial activated carbon (Wang and Zhu, 2007). Results for OPAC suggest that the mechanism responsible for the adsorption of MB and RhB may be more related to textural properties and dispersion interactions between the aromatic rings in the dyes molecules and the graphitic-like layers of the orange peel-based carbon rather than to electrostatic interactions with the surface groups onto OPAC. Based on present results, a value of pH 7 was selected for the batch and continuous experiments as the best one for MB adsorption, considering the differences in RhB removal between pH 4 and 7 almost negligible.

Kinetic data for the adsorption of both dyes are presented in Fig. 5. As seen, adsorption was initially very fast for both dyes and slowed gradually as equilibrium was attained, a consequence of the reduction of the available active sites onto OPAC. A pseudo-second-order rate model (Ho, 2006) was applied in order to describe the adsorption kinetics:

$$q_t = \frac{q_{\text{eH}}^2 k_H t}{1 + q_{\text{eH}} k_H t} \quad (3)$$

where q_t is the amount of dye adsorbed at any time t per unit mass of adsorbent [mmol/g], k_H , the rate constant of adsorption [g/mmol min], and q_{eH} , the amount of dye adsorbed at equilibrium per unit mass of adsorbent [mmol/g]. Model parameters for the adsorption of both dyes are summarized in Table 3. They were estimated by non-linear regression analysis for a 5% significance level, by minimizing the following objective function (O.F.):

$$\text{O.F.} = \sum (q_{\text{exp}} - q_{\text{mod}})^2 \quad (4)$$

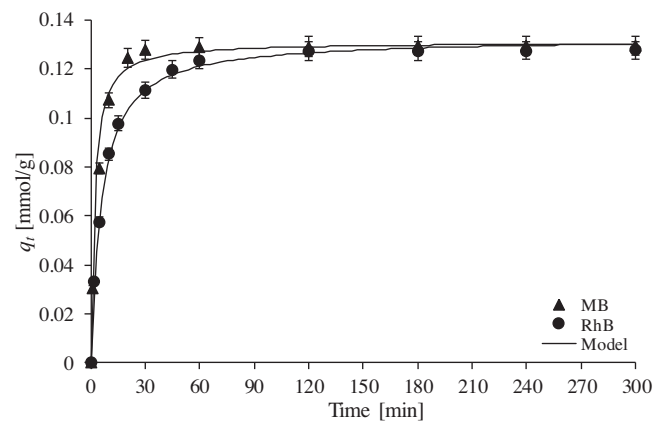


Fig. 5. Kinetic data for adsorption from single solutions of methylene blue (MB) and rhodamine B (RhB) onto OPAC. Comparison between experimental data (points) and predictions of the pseudo-second-order rate model (lines). $C_0 = 0.21 \text{ mmol/L}$ at pH 7; dose: $0.2 \text{ g}/100 \text{ mL}$.

Table 3

Estimated parameters of the pseudo-second-order kinetic model for the adsorption of methylene blue (MB) and rhodamine B (RhB) onto OPAC.

Model parameters	MB	RhB
q_{eH} [mmol/g]	0.131	0.133
k_H [g/mmol min]	4.20	1.30
r^2	0.971	0.998

As it may be appreciated from Fig. 5 and Table 3, the kinetic model enabled to properly describe the experimental data with high correlation coefficients for both dyes, especially for RhB. The rate constant estimated for MB was three times higher than for RhB adsorption. Fast adsorption rates using mesoporous carbons are mainly attributed to the easy access of dye molecules into the mesopores (Hao et al., 2010). The MB molecule has a minimum molecular cross-section of about 0.8 nm, and it has been estimated that the minimum pore diameter it can enter is 1.3 nm; therefore, it can only enter the largest micropores (supermicropores) and mostly be adsorbed in mesopores (Yang and Qiu, 2011). On the other hand, RhB can access exclusively the mesopores, not only because of its bigger size but, additionally, because aggregation of the zwitterionic form of RhB occurs at $\text{pH} > 4$ (Fernandez et al., 2010; Gad and El Sayed, 2009).

Experimental isotherms for the adsorption of MB and RhB onto OPAC obtained from single dye-solutions are shown in Fig. 6a and b, respectively. Three different adsorption models were comparatively applied to data fitting. The Langmuir model is described by the following equation:

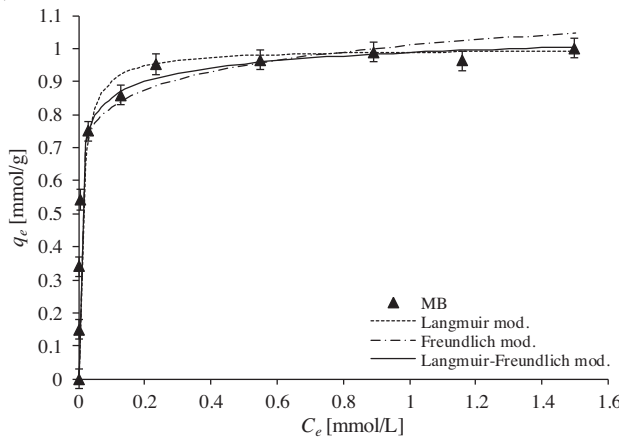
$$q_e = \frac{k_L q_{\text{mL}} C_e}{1 + k_L C_e} \quad (5)$$

where q_e is the molar amount of the dye adsorbed at equilibrium per unit mass of adsorbent [mmol/g], k_L , the Langmuir constant related to the energy of adsorption [L/mmol] and q_{mL} , the maximum amount of adsorption corresponding to complete monolayer surface coverage [mmol/g]. The Freundlich model is represented by:

$$q_e = k_F C_e^{n_F} \quad (6)$$

where k_F and n_F are the Freundlich isotherm constants related to adsorption capacity and intensity, respectively. Finally, a

(a)



(b)

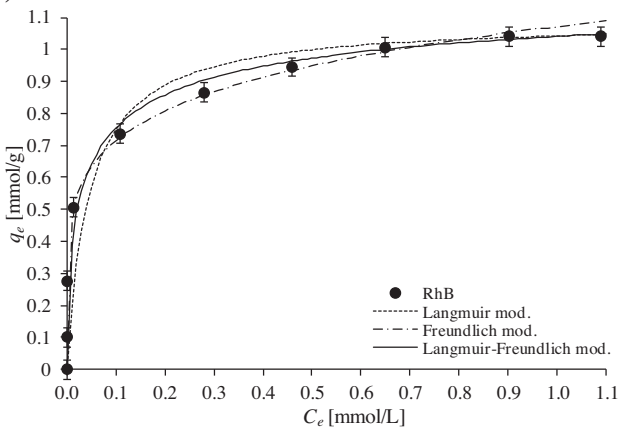


Fig. 6. Equilibrium isotherms for (a) methylene blue (MB) and (b) rhodamine B (RhB) onto OPAC. Comparison between the experimental data (points) and predictions of the Langmuir, Freundlich and Langmuir–Freundlich models (lines). Dose: 0.04 g/100 mL.

combination of the two previous models, best known as the Langmuir–Freundlich equation (Janoš et al., 2009) was applied:

$$q_e = \frac{k_{LF} q_{mLF} C_e^{n_{LF}}}{1 + k_{LF} C_e^{n_{LF}}} \quad (7)$$

where q_{mLF} is the maximum amount of adsorption [mmol/g], k_{LF} , the Langmuir–Freundlich constant [L/mmol], and n_{LF} , an additional parameter of the system's heterogeneity. Estimated characteristic parameters of the models for the adsorption of MB and RhB onto OPAC are presented in Table 4. They were also estimated by non-linear regression analysis for a 5% significance level, as detailed before (Eq. (4)).

As it may be appreciated in Fig. 6a and b and Table 4, the Freundlich and Langmuir–Freundlich models enabled to represent the experimental data for both systems appropriately, reinforcing the idea of a heterogeneous material with energetically non-equivalent surface sites, where a multilayer adsorption can occur. The Langmuir model led to a less adequate description of the results, as revealed by lower values of r^2 . Regardless of the model applied, adsorption capacities of the dyes using OPAC were quite similar to each other, with a slightly higher adsorption capacity for RhB than for MB in the three cases. However, a large difference in the adsorption intensity arose, supported by the k_L and k_{LF} values, which points to stronger interaction forces between OPAC surface and MB in comparison with RhB. The maximum monolayer

Table 4

Model parameters estimated for the adsorption isotherms of methylene blue (MB) and rhodamine B (RhB) onto OPAC.

	MB	RhB
Langmuir parameters		
q_{mL} [mmol/g]	1.00	1.09
k_L [L/mmol]	91.1	22.0
r^2	0.835	0.876
Freundlich parameters		
n_F	0.09	0.18
k_F [(mmol/g)(L/mmol) n_F]	1.01	1.07
r^2	0.962	0.995
Langmuir–Freundlich parameters		
q_{mLF} [mmol/g]	1.14	1.23
k_{LF} [(L/mmol) n_{LF}]	6.7	5.5
n_{LF}	0.35	0.55
r^2	0.996	0.972

adsorption capacities of OPAC for both dyes, depicted by the q_{mL} values, were higher compared to those reported in literature for ACs derived from orange peels (Dutta et al., 2011; Okeola and Odebummi, 2010) and comparable to the highest values listed in the review by Rafatullah et al. (2010) for ACs derived from other agricultural and industrial wastes; whereas adsorption capacities for RhB were higher than those of ACs derived from bagasse pith (Gad and El Sayed, 2009) and tire wastes (Li et al., 2010) and similar to that derived from *Polygonum orientale* Linn. (Wang et al., 2010).

Experimental isotherms for the adsorption of MB and RhB obtained from binary solutions are depicted in Fig. 7a and b, respectively. The shapes of the isotherms were similar to those obtained from single-dye solutions. However, reduced adsorption capacities for both dyes were attained, suggesting possible competitive effects between the dyes. This can be attributed to several factors including: interaction between the dyes in solution, change of the adsorbent surface charge as a consequence of adsorption and displacement effects due to competition between the dyes for the active sites on the carbon surface (Okeola and Odebummi, 2010). Three different models were applied to describe the binary experimental isotherms. The Langmuir–Freundlich model for single-component isotherms, described by Eq. (7), was used. Besides, a multi-component extended Langmuir model was also applied. This model assumes competitive interactions (Kumar et al., 2008) and it is represented by the following expressions:

$$q_{e,1} = \frac{q_{mEL,1} k_{EL,1} C_{e,1}}{1 + k_{EL,1} C_{e,1} + k_{EL,2} C_{e,2}} \quad (8)$$

$$q_{e,2} = \frac{q_{mEL,2} k_{EL,2} C_{e,2}}{1 + k_{EL,1} C_{e,1} + k_{EL,2} C_{e,2}} \quad (9)$$

where 1 and 2 represent MB and RhB, respectively, q_e , the amount of each dye adsorbed at equilibrium per unit mass of adsorbent [mmol/g], C_e , the equilibrium dye concentration in solution [mmol/L], q_{mEL} , the maximum adsorption capacity [mmol/g] and k_{EL} , an affinity constant [L/mmol]. Also, the Sheindorf–Reuhn–Sheintuch (SRS) model (Sheindorf et al., 1981), a Freundlich-type isotherm for multi-component adsorption, was applied. Model equations are given by:

$$q_{e,1} = k_{F,1} C_{e,1} (C_{e,1} + a_1 C_{e,2})^{n_{F,1}-1} \quad (10)$$

$$q_{e,2} = k_{F,2} C_{e,2} (C_{e,2} + a_2 C_{e,1})^{n_{F,2}-1} \quad (11)$$

where k_F and n_F are the Freundlich model constants obtained for each dye from the single-dye solution isotherms (reported in Table 4), and a_1 and a_2 , competition coefficients for the adsorption of one dye in the presence of the other, estimated from the binary data. The models parameters, estimated by non-linear regression analysis, are presented in Table 5. The results presented

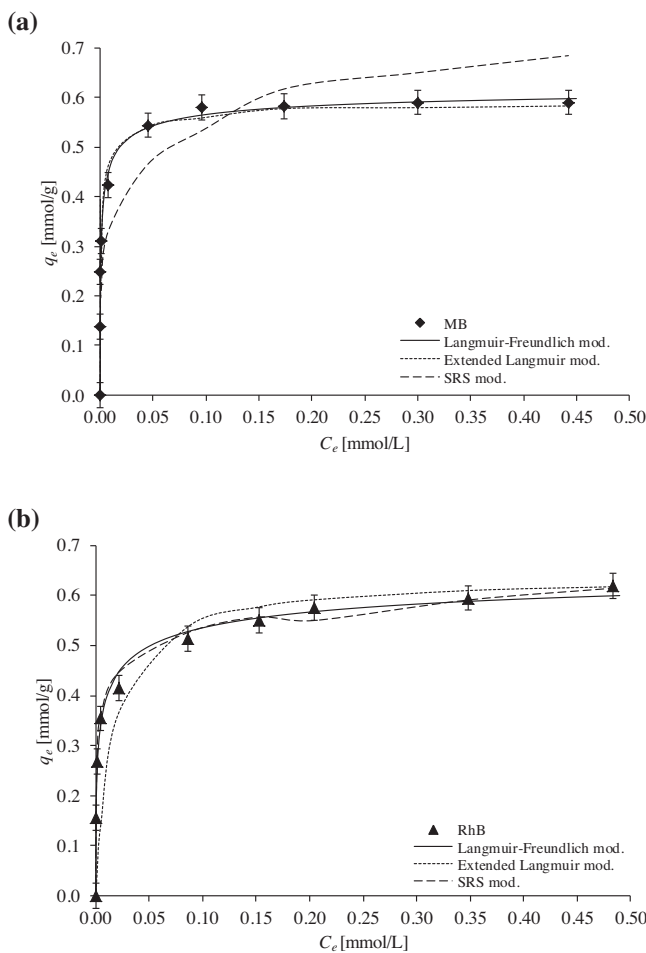


Fig. 7. Equilibrium isotherms for (a) methylene blue (MB) and (b) rhodamine B (RhB) onto OPAC. Comparison between the experimental data (points) and predictions of the Langmuir-Freundlich, extended Langmuir and SRS models (lines). Dose: 0.04 g/100 mL.

in Fig. 7a and b and Table 5 show that the single-component Langmuir-Freundlich model (Eq. (7)) enabled to the best representation of the experimental isotherms for both dyes from the binary system. Other authors have also described satisfactorily the adsorption isotherms from multi-component solutions applying single-component models (Al-Degs et al., 2007; Kumar et al., 2008). Neither of the dyes had a stronger inhibitory effect over the other or was predominantly adsorbed onto OPAC as they both reduced their

Table 5
Model parameters estimated for the adsorption isotherms of methylene blue (MB) and rhodamine B (RhB) obtained from binary solutions, onto OPAC.

	MB	RhB
Langmuir-Freundlich parameters		
q_{mLF} [mmol/g]	0.63	0.69
k_{LF} [(L/mmol) nLF]	26.4	8.9
n_{LF}	0.49	0.41
r^2	0.990	0.990
Extended Langmuir parameters		
q_{mEL}	0.63	0.64
k_{EL} [L/mmol]	920.0	72.0
r^2	0.976	0.760
SRS parameters		
a_1	0.38	–
a_2	–	0.74
r^2	0.818	0.984

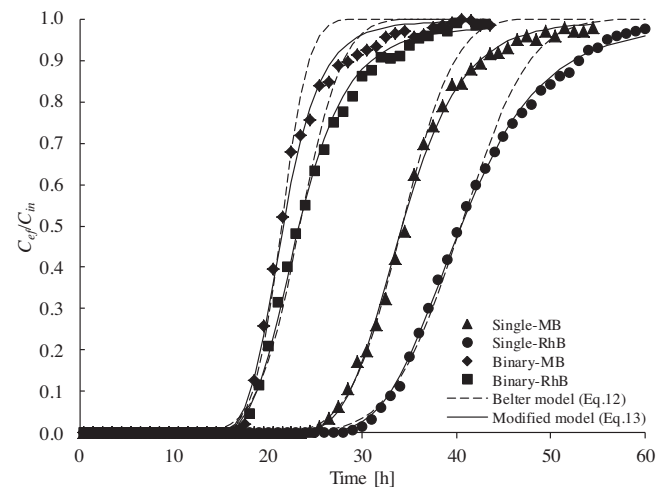


Fig. 8. Breakthrough curves obtained for dynamic adsorption of methylene blue (MB) and rhodamine B (RhB) onto OPAC from single and binary dye solutions. Comparison between the experimental data (points) and the predictions of the mathematical models given by Eqs. (12) and (13) (lines). $C_{in} = 0.21$ mmol/L at pH 7. Load of adsorbent: 6 g. Flow rate: 11 mL/min.

adsorption in a similar proportion (~60%) with respect to those estimated from the single solutions (Table 4). Stronger interaction forces were estimated between OPAC surface and MB, in agreement with the results obtained for single-dye solutions. Similar maximum adsorption capacities and stronger interaction forces with MB were also estimated by the extended Langmuir model, although a less appropriate description of the experimental isotherm for RhB adsorption was obtained. The SRS model was unable to fit the data for MB adsorption.

3.3. Dynamic adsorption of the dyes onto OPAC

Comparisons for dynamic adsorption of MB and RhB onto OPAC from single and binary dyes solutions are illustrated in Fig. 8. Breakthrough curves in the figure are expressed in terms of normalized concentration, defined as the ratio of effluent dye concentration to influent dye concentration (C_{ef}/C_{in}), as a function of time (t). As it can be observed, breakthrough curves from the binary solution maintained the typical S-shapes and the tailing near t_e , in agreement with those obtained for the single-dye solutions. Breakthrough for RhB occurred at more prolonged times (t_b), indicating a better removal performance even in the presence of the other dye. In multi-component systems, adsorption may be greater for the larger molecules, and it has been reported to be a direct function of the molecular dimensions of the adsorbate and inversely proportional to its solubility and pKa (Attia et al., 2003). Moreover, at the pH selected for the adsorption experiments, the aggregation of the zwitterionic form of RhB may generate dimmers with lower net charge which could benefit the interaction between the dye and the graphitic-like structures of the activated carbon.

Performance parameters for the breakthrough curves, obtained from single and binary solutions, were calculated as earlier detailed in the article by Fernandez et al. (2010). They are listed in Table 6. Column adsorption capacities (q_c) from single and binary solutions were inferior to those obtained from batch experiments (75–90%). This result is usually attributed to the insufficient contact time between the solute and the adsorbent in the column (Tan et al., 2008b). The q_c values for each individual dye, determined from the breakthrough curves obtained with the binary solution, were lower than those determined with the single-dye solutions. This substantial reduction suggests that the adsorption of both MB and RhB mainly occurs in the mesopores of OPAC. However, taking

Table 6

Performance and estimated models parameters (t_0 and σ) for the adsorption of methylene blue (MB) and rhodamine B (RhB) by OPAC from single and binary dye solutions in continuous mode. $C_m = 0.21 \text{ mmol/L}$ of each dye, at pH 7. Load of adsorbent: 6 g. Flow rate: 11 mL/min.

	Single solutions		Binary solution	
	MB	RhB	MB	RhB
Performance parameters				
t_b^a [h]	27.0	31.6	17.8	18.5
t_e^b [h]	46.5	56.0	32.3	36.5
L_m^c [cm]	4.9	5.2	5.4	5.9
q_c^d [mmol/g]	0.88	0.98	0.55	0.57
Belter model parameters				
t_0 [h]	34.2	40.5	21.4	23.4
σ	0.13	0.14	0.11	0.15
r^2	0.993	0.982	0.980	0.986
Modified model parameters				
t_0 [h]	34.2	40.5	21.6	23.3
σ	0.054	0.063	0.055	0.068
r^2	0.999	0.999	0.996	0.998

^a Breakthrough time.

^b Exhaustion time.

^c Length of the mass transfer zone.

^d Dye uptake at exhaustion.

into account the smaller size and flattened shape of MB, some MB molecules may have access to the supermicropores (1–2 nm) of OPAC, which are inaccessible to RhB molecules.

In order to represent the experimental breakthrough curves, two empirical models were applied: the two-parameter model proposed by Belter (Eq. (12)) and its modification (Eq. (13)); the latter is described by a similar expression as those presented by Chu (2004) for curves with asymmetric shape, and does not introduce any additional parameter to the original model. Models equations are respectively represented by:

$$\frac{C_{\text{ef}}}{C_{\text{in}}} = \frac{1}{2} \left(1 + \text{erf} \left[\frac{(t - t_0)}{\sqrt{2}\sigma t_0} \right] \right) \quad (12)$$

$$\frac{C_{\text{ef}}}{C_{\text{in}}} = \frac{1}{2} \left(1 + \text{erf} \left[\frac{(t - t_0) \exp(-t/t_0)}{\sqrt{2}\sigma t_0} \right] \right) \quad (13)$$

where $\text{erf}[x]$ is the error function of x , t_0 , the time at which the dye effluent concentration is half the dye influent concentration [h], and σ , the standard deviation of the linear part of the curve which is a measure of the slope of the breakthrough curve. The models parameters, t_0 and σ , were estimated by non-linear regression analysis and are also summarized in Table 6. The results in Fig. 8 and Table 6 show that both models accurately described the experimental breakthrough curves for the adsorption of both dyes, from single and binary solutions up to $C_{\text{ef}}/C_{\text{in}} \sim 0.7$, with almost the same values of t_0 predicted by both models. While the Belter model overestimated the sharpness of the breakthrough curves, the modified model was able to describe properly the entire experimental curves. The t_0 value for each dye from the binary solution was reduced approximately 60% in comparison to those from the single-dye solutions. The effect of the tailing of the curves obtained with the binary solution caused a slightly more pronounced asymmetry. It might lead to shorter mass transfer zones for the adsorption of MB and RhB from the single-dye solutions, as reflected in the smaller L_m and σ values calculated (Table 6), in comparison to those from the binary solution. The broader tailing is probably related to slower intraparticle diffusion within the pores of the activated carbon (Chu, 2004).

4. Conclusions

Orange peels were found to be a suitable material for the preparation of activated carbon by H_3PO_4 acid activation, showing potentialities for basic dyes removal. The developed activated carbon showed high adsorption capacity for both MB and RhB. Fast adsorption kinetics of both dyes was successfully described by a pseudo-second-order rate model. Low dependency of dyes adsorption on solution pH, which is a very desirable feature in real wastewater treatment, suggests an adsorption mechanism mainly related to the textural properties and dispersion interactions of the orange peel-based carbon. Single and binary isotherms were represented by several models, with the single-component Langmuir–Freundlich model being the most satisfactory one. Tailed-shaped breakthrough curves from single and binary dye solutions were successfully fitted by a modified two-parameter model. The batch and dynamic experiments using binary dyes solutions allowed the identification of a reduced adsorption of both dyes, pointing to a certain degree of competition for the active sites in the mesopores of the developed carbon.

Acknowledgements

The authors gratefully acknowledge Consejo Nacional de Investigaciones Científicas y Técnicas (CONICET), Fondo para la Investigación Científica y Tecnológica–Agencia Nacional de Promoción Científica y Tecnológica (FONCYT-ANPCYT) and Universidad de Buenos Aires (UBA) from Argentina, for their financial support, and Ricardo Martín Ramírez for language assistance.

References

- Agustí, M., Almela, V., Juan, M., Alferez, F., Tadeo, F.R., Zacarías, F., 2001. Histological and physiological characterization of rind breakdown of 'Navelate' sweet orange. *Ann. Bot.* 88, 415–422.
- Al-Degs, Y., Khraisheh, M.A.M., Allen, S.J., Ahmad, M.N., Walker, G.M., 2007. Competitive adsorption of reactive dyes from solution: equilibrium isotherm studies in single and multisolute systems. *Chem. Eng. J.* 128, 163–167.
- Attia, A.A., Girgis, B.S., Khedr, S.A., 2003. Capacity of activated carbon derived from pistachio shells by H_3PO_4 in the removal of dyes and phenolics. *J. Chem. Technol. Biotechnol.* 78, 611–619.
- Basso, M.C., Cerrella, E.G., Cukierman, A.L., 2002. Activated carbons developed from a rapidly renewable biosource for removal of cadmium(II) and nickel(II) ions from dilute aqueous solutions. *Ind. Eng. Chem. Res.* 41, 180–189.
- Benadjemia, M., Millière, L., Reinert, L., Benderdouche, N., Duclaux, L., 2011. Preparation, characterization and Methylene Blue adsorption of phosphoric acid activated carbons from globe artichoke leaves. *Fuel Process. Technol.* 92, 1203–1212.
- Chu, K.H., 2004. Improved fixed bed models for metal biosorption. *Chem. Eng. J.* 97, 233–239.
- de Celis, J., Amadeo, N.E., Cukierman, A.L., 2009. In situ modification of activated carbons developed from a native invasive wood on removal of trace toxic metals from wastewater. *J. Hazard. Mater.* 161, 217–223.
- Deniz, F., Karaman, S., Saygideger, S.D., 2011. Biosorption of a model basic dye onto *Pinus brutia* Ten.: evaluating of equilibrium, kinetic and thermodynamic data. *Desalination* 270, 199–205.
- Dutta, S., Bhattacharyya, A., Ganguly, A., Gupta, S., Basu, S., 2011. Application of response surface methodology for preparation of flow-cost adsorbent from citrus fruit peel and for removal of Methylene Blue. *Desalination* 275, 26–36.
- El Nemr, A., Abdelwahab, O., El-Sikaily, A., Khaled, A., 2009. Removal of direct blue-86 from aqueous solution by new activated carbon developed from orange peel. *J. Hazard. Mater.* 161, 102–110.
- Feng, N., Guo, X., Liang, S., 2009. Adsorption study of copper (II) by chemically modified orange peel. *J. Hazard. Mater.* 164, 1286–1292.
- Fernandez, M.E., Nunell, G.V., Bonelli, P.R., Cukierman, A.L., 2010. Effectiveness of *Cupressus sempervirens* cones as biosorbent for the removal of basic dyes from aqueous solutions in batch and dynamic modes. *Bioresour. Technol.* 101, 9500–9507.
- Foo, K.Y., Hameed, B.H., 2012. Preparation, characterization and evaluation of adsorptive properties of orange peel based activated carbon via microwave induced K_2CO_3 activation. *Bioresour. Technol.* 104, 679–686.
- Gad, H.M.H., El Sayed, A.A., 2009. Activated carbon from agricultural by-products for the removal of Rhodamine-B from aqueous solution. *J. Hazard. Mater.* 168, 1070–1081.

- Garg, V.K., Amita, M., Kumar, R., Gupta, R., 2004. Basic dye (methylene blue) removal from simulated wastewater by adsorption using Indian Rosewood sawdust: a timber industry waste. *Dyes Pigments* 63, 243–250.
- Hao, G.P., Li, W.C., Wang, S., Zhang, S., Lu, A.H., 2010. Tubular structured ordered mesoporous carbon as an efficient sorbent for the removal of dyes from aqueous solutions. *Carbon* 48, 3330–3339.
- Ho, Y.S., 2006. Review of second-order models for adsorption systems. *J. Hazard. Mater.* 136, 681–689.
- Hu, Z., Srinivasan, M.P., Ni, Y., 2001. Novel activation process for preparing highly microporous and mesoporous activated carbons. *Carbon* 39, 877–886.
- Janaki, V., Vijayaraghavan, K., Ramasamy, A.K., Lee, K.J., Oh, B.T., Kamala-Kannan, S., 2012. Competitive adsorption of reactive Orange 16 and reactive Brilliant Blue R on polyaniiline/bacterial extracellular polysaccharides composite – a novel eco-friendly polymer. *J. Hazard. Mater.* 241–242, 110–117.
- Janoš, P., Coskun, S., Pilařová, V., Rejnek, J., 2009. Removal of basic (methylene blue) and acid (eggacid orange) dyes from waters by sorption on chemically treated wood shavings. *Bioresour. Technol.* 100, 1450–1453.
- Kumar, D., Singh, A., Gaur, J.P., 2008. Mono-component versus binary isotherm models for Cu(II) and Pb(II) sorption from binary metal solution by the green alga *Pithophora oedogonia*. *Bioresour. Technol.* 99, 8280–8287.
- Li, L., Liu, S., Zhu, T., 2010. Application of activated carbon derived from scrap tires for adsorption of Rhodamine B. *J. Environ. Sci.* 22 (8), 1273–1280.
- Lodeiro, P., Herrero, R., Sastre de Vicente, M.E., 2006. The use of protonated *Sargassum muticum* as biosorbent for cadmium removal in a fixed-bed column. *J. Hazard. Mater. B* 137, 244–253.
- Nunell, G.V., Fernandez, M.E., Bonelli, P.R., Cukierman, A.L., 2012. Conversion of biomass from an invasive species into activated carbons for removal of nitrate from wastewater. *Biomass Bioenergy* 44, 87–95.
- Okeola, F.O., Odebutunmi, E.O., 2010. Freundlich and Langmuir isotherms parameters for adsorption of Methylene Blue by activated carbon derived from agrowastes. *Adv. Nat. Appl. Sci.* 4 (3), 281–288.
- Puziy, A.M., Poddubnaya, O.I., Martínez-Alonso, A., Castro-Muñiz, A., Suárez-García, F., Tascón, J.M.D., 2007. Oxygen and phosphorus enriched carbons from lignocellulosic material. *Carbon* 45, 1941–1950.
- Rafatullah, M., Sulaiman, O., Hashim, R., Ahmad, A., 2010. Adsorption of methylene blue on low-cost adsorbents: a review. *J. Hazard. Mater.* 177, 70–80.
- Rodríguez Couto, S., 2009. Dye removal by immobilised fungi. *Biotechnol. Adv.* 27, 227–235.
- Sangwichien, C., Aranovich, G.L., Donohue, M.D., 2002. Density functional theory predictions of adsorption isotherms with hysteresis loops. *Colloids Surf. A* 206, 313–320.
- Sheindorf, C.H., Rebhun, M., Sheintuch, M., 1981. A Freundlich-type multicomponent isotherm. *J. Colloid Interface Sci.* 79 (1), 136–142.
- Siles López, J.A., Li, Q., Thompson, I.P., 2010. Biorefinery of waste orange peel. *Crit. Rev. Biotechnol.* 30 (1), 63–69.
- Tan, I.A.W., Ahmad, A.L., Hameed, B.H., 2008a. Enhancement of basic dye adsorption uptake from aqueous solutions using chemically modified oil palm shell activated carbon. *Colloids Surf. A* 318, 88–96.
- Tan, I.A.W., Ahmad, A.L., Hameed, B.H., 2008b. Adsorption of basic dye using activated carbon prepared from oil palm shell: batch and fixed bed studies. *Desalination* 225, 13–28.
- Thirumavalavan, M., Lai, Y.L., Lee, J.F., 2011. Fourier transform infrared spectroscopic analysis of fruit peels before and after the adsorption of heavy metal ions from aqueous solution. *J. Chem. Eng. Data* 56, 2249–2255.
- Wang, L., Zhang, J., Zhao, R., Li, C., Li, Y., Zhang, C., 2010. Adsorption of basic dyes on activated carbon prepared from *Polygonum orientale* Linn: equilibrium, kinetic and thermodynamic studies. *Desalination* 254, 68–74.
- Wang, S., Zhu, Z.H., 2007. Effects of acidic treatment of activated carbons on dye adsorption. *Dyes Pigments* 75, 306–314.
- Wawrzkiecicz, M., Hubicki, Z., 2009. Removal of tartrazine from aqueous solutions by strongly basic polystyrene anion exchange resins. *J. Hazard. Mater.* 164, 502–509.
- Yang, J., Qiu, K., 2011. Experimental design to optimize the preparation of activated carbons from herb residues by vacuum and traditional ZnCl₂ chemical activation. *Ind. Eng. Chem. Res.* 50, 4057–4064.